Observations of *PKKP* Precursors Used to Estimate Small-Scale Topography on the Core-Mantle Boundary

Paul S. Earle and Peter M. Shearer

Stacks of global seismic data reveal the time and distance dependence of high-frequency (1-hertz) precursors to the seismic phase *PKKP*. Synthetic seismogram modeling shows that scattering from random small-scale topography at the *PKKP* core-mantle–boundary reflection point generates precursory arrivals similar to those seen in the data. Models with a root mean square core-mantle–boundary topography of 250 to 350 meters and correlation length of 7 to 10 kilometers explain the main features of the data. However, a systematic range-dependent misfit between observed and predicted precursor power suggests that inner core scattering may contribute to the precursors.

The core-mantle boundary (CMB) marks the most significant change in material properties within Earth. At a depth of 2889 km, energy passing from the solid silicate perovskite mantle to the liquid iron outer core encounters a 78% density increase, a 41% drop in compressional wave velocity, and a complete barrier to shear wave propagation (*1*). Separating materials that vary in viscosity by 20 to 24 orders of magnitude, the CMB divides two vastly different convective regimes. Knowledge of its topography would increase understanding of several aspects of Earth science, including the physical coupling between the outer core and mantle, thermal and chemical diffusion times across the boundary, the behavior of the magnetic field, and the chemical composition of the lowermost mantle (*2*). Topography on the CMB, like that on Earth's surface, likely exists on many length scales. At scales of thousands of kilometers, early attempts to map CMB topography with the use of travel times of core-reflected and -refracted phases suggested relief of ±6 km (*3*), but later studies indicated that these features were not reliably resolved (*4*), in part because of the problem of separating the effects of mantle velocity heterogeneity from CMB structure. Deterministic mapping of topography at smaller horizontal scale lengths (on the order of 10 km) is even more difficult, given the limited spatial sampling of the CMB by teleseismic energy. However, by examining high-frequency scattered energy or the pulse distortion of short-period body waves, it is possible to constrain the statistical properties of short-wavelength CMB topography (*5*, *6*).

The observed onset times of high-frequency precursors to the direct core phase PKP can be interpreted as scattering from small-scale CMB topography (*7*, *8*) but can equally be explained by volumetric scattering from velocity heterogeneity in the lowermost mantle (*8*). In principle, more direct constraints on CMB topography can be obtained from observations of the underside CMB reflected phase PKKP (Fig. 1A). Because PKKP is a maximum travel time phase with respect to perturbations of its CMB reflection point, energy scattered from a rough CMB will precede the PKKP arrival. Forward scattering due to mantle heterogeneity generates PKKP precursors only at ranges beyond 125° distance from source to receiver (Fig. 1B). Thus, at ranges less than 125°, precursors to PKKP offer a unique opportunity to observe CMB scattering free from the effects of mantle and crustal heterogeneity.

However, the small-amplitude PKKP precursors are hard to resolve on individual seismograms. Previous observations using beam-forming methods on seismic arrays noted PKKP precursors near 60° (*9*) and between 80° and 106° (*6*), with the latter observation suggesting a CMB with average small-scale topography of 100 to 200 m. Because these results have been restricted to a handful of records and a limited number of source and receiver locations, they cannot reliably constrain the global extent of a rough CMB or resolve the time and range dependence of the precursors. Here we analyze thousands of seismograms from the global networks and apply a stacking technique that images PKKP precursors at ranges between 80° and 112°. We use these observations to place upper bounds on small-scale CMB topography and suggest the existence of scattering from the inner core.

To begin our analysis, we obtained 25,047 broadband seismograms from the Global Seismic Network (GSN) at ranges from 80° to 120°, which are available through an online archive maintained by the Incorporated Research Institutions in Seismology (IRIS) (*10*). Next, we selected a subset of the data with the clearest PKKP arrivals. After bandpass filtering (0.7 to 2.5 Hz), traces with a *PKKPbc* signal-to-noise

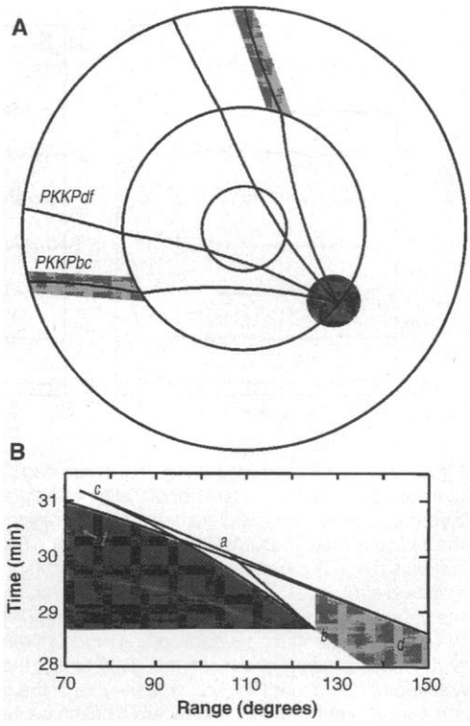

Fig. 1. (**A**) Cross section of Earth showing the mantle, liquid outer core, solid inner core, and example ray paths for *PKKPbc* and *PKKPdf*. (**B**) The *PKKP* travel time curves, with different branches labeled in lowercase italics. The branches of *PKKP* all have a single CMB reflection point and turn at different depths within Earth. *PKKPab* turns in the upper portion of the outer core, *PKKPbc* samples deeper in the outer core, *PKKPcd* reflects twice from the top of the ICB, and *PKKPdf* transects the outer core and has two legs in the inner core. The light and dark gray regions in (B) indicate the time and distance windows at which scattered *PKKP* energy arrives before any branch of *PKKP*. Forward scattering along the mantle legs of *PKKPbc* [the region shown as light gray in (A)] and *PKKPab* can generate precursors only at distance ranges greater than 125° [light gray region in (B)]. Forward scattering of this type produces precursors to *PKPdf* (a core phase with no underside CMB reflection), which have been extensively studied and suggest the existence of small-scale heterogeneities in the mantle (*26*). Single forward scattering of the *df* branch of *PKKP* in the mantle will not produce precursors. At distance ranges less than 125° [dark gray region in (B)], one can observe backscattered *PKKP* energy from a rough CMB [dark gray region in (A)] that is free from contamination by mantle and crustal heterogeneity. This unique window to the CMB was used in our study.

Institute of Geophysics and Planetary Physics, Scripps Institution of Oceanography, University of California, San Diego, La Jolla, CA 92093–0225, USA.

ratio (SNR) less than 1.5 were discarded. By restricting our study to high frequencies [where *PKKP* is most easily observed (*11*)], we focused on short-wavelength scattering and avoided contamination from the low-frequency *S* coda. Seismograms with nonstationary noise preceding *PKKPbc* were removed (*12*). The final data set consisted of 1856 vertical-component seismograms and provided good coverage of the CMB (*13*).

The small-amplitude precursory wave trains were not observed on single seismograms. To enhance their visibility, we employed the following stacking technique: (i) The envelope function (positive outline) (*14*) was calculated for each trace. This avoided cancellation of the incoherent scattered arrivals when they were stacked. (ii) The envelope function was squared to convert amplitude to power and make the stacking procedure linear. (iii) We subtracted the average noise (*15*) and normalized to the maximum *PKKPbc* amplitude (*16*) to account for varying signal and noise levels between traces. (iv) Weights proportional to the STN of the *PKKPbc* arrival were assigned to the traces (*17*). (v) Finally, the data were aligned on the predicted *PKKPbc* onset and binned in range (*18*) and time (4° × 4 s), and the weighted average was calculated and plotted.

The resulting stack imaged energy arriving up to 60 s before *PKKPbc* (Fig. 2A). The precursors' power, relative to *PKKPbc*, generally increased with time, and at longer ranges the precursors initiated closer to the main arrival. Their maximum relative power was similar in the distance range 80° to 112°. Outside this range, *PKKPbc* provided a poor reference for stacking; at distances less than 80° its amplitude was too small, and for distances greater than 112° it was often difficult to separate the *PKKPab* and *PKKPbc* arrivals.

Error bounds were computed for the precursory power levels by repeating the stack many times on data randomly selected from the original seismograms (*19*). The precursor power levels were nonzero to better than 95% confidence over the distance range 80° to 112° (Fig. 2B). As a test for possible biases in the stacking procedure, we repeated the stack using the same seismograms but with *P* as a reference phase. *P* is a minimum travel time phase; thus, it will precede any energy scattered along its path. The *P* stack (Fig. 2C) showed no coherent energy arriving before its theoretical onset time, which indicates that the wave train preceding *PKKPbc* is real and not an artifact of the stacking method.

Because the underside *PKKP* reflection point on the CMB is a maximum time point with respect to lateral variations of the reflection point, small-scale CMB topography provides a likely explanation for the observed precursors (6, 9). We computed the effect of CMB topography on *PKKP* by applying Kirchhoff theory to models of random small-scale topography on the boundary. Based on Huygen's principle, Kirchhoff theory is widely used to study scattering from rough surfaces and has been experimentally and theoretically verified (*20*). It neglects the effects of multiple scattering, but this appears reasonable given the small amplitude of the precursors relative to the *PKKP* arrivals.

The response for a specified topography at a given range is calculated by propagating the wave field to the CMB with ray theory, evaluating the surface Kirchhoff integral (*21*), and then propagating the solution back to the surface. The synthetic calculations include scattering between all branches of *PKKP* (*ab*, *bc*, *cd*, and *df*). To obtain an average theoretical scattering envelope for comparison with the data, we applied our stacking method to synthetic seismograms calculated from unique realizations of CMB topography having identical statistical properties. The stacked responses were then convolved with a data-derived source-time function and shifted in time to line up with the observed *PKKPbc* onset (the maximum shift is 2.5 s).

The calculation of the theoretical envelope involves many factors, including geometrical spreading terms, reflection and transmission coefficients at the CMB and other interfaces, attenuation (particularly within the inner core for the *df* branch), and the CMB topography model. However, by assuming a reference one-dimensional Earth model (1) and random CMB topography with a Gaussian autocorrelation function, only two free parameters remain: the topography correlation length λ and root mean square (rms) amplitude σ. The correlation length provides a measure of the typical horizontal scale length of the peaks and depressions in the assumed topography. To find the best fitting model to the *PKKP* precursor observations, we explored this restricted model space using a simple grid search approach (*22*).

The preferred model was obtained for λ = 8 km and σ = 300 m (Fig. 2B). However, values of λ between 7 and 10 km and values of σ between 250 and 350 m produce fits that are almost as good (*23*). The Kirchhoff synthetics share many features with the data: The scattered energy is observed well before the onset of *PKKP*, the power of the precursor wave train increases as it approaches *PKKP*, and the onset of the scattering envelope initiates closer to *PKKP* for larger ranges. Topography on the CMB is capable of explaining much of the observed signal. However, a systematic misfit as a function of range between the synthetics and the observed precursors suggests that there may be difficulties with this simple model.

Synthetic envelopes for all correlation lengths and rms amplitudes that we considered increase in relative power with increasing range, whereas no such trend is observed in the data. Thus, our best fitting

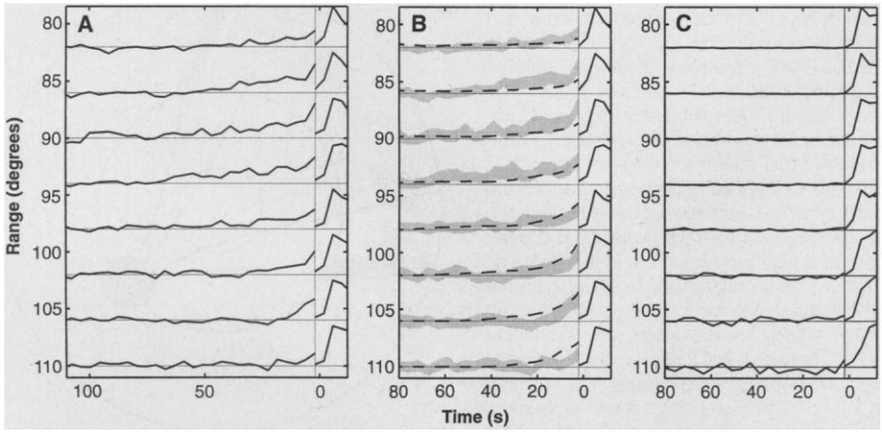

Fig. 2. Data stacks and predictions of our preferred (*23*) CMB topography model. To aid in visualization, all traces are magnified by a factor of 8 at times before −2 s in each plot. The thin horizontal lines indicate zero values. Each trace was generated by averaging data over a distance range of 4° and is plotted in the middle of that range. (**A**) Data stack aligned on *PKKPbc*. Energy is evident preceding *PKKPbc* in the distance range 80° to 112°. (**B**) Predicted precursor power levels (dashed lines) compared to the ±2 standard error limits of the observations (gray shaded regions). The error estimates were obtained from the data using a bootstrap resampling technique (*19*). The theoretical predictions were calculated with the use of Kirchhoff theory applied to a model of random CMB topography with rms height of 300 m and horizontal scale length of 8 km. (**C**) A test of the stacking method. Waveforms were aligned and stacked on the direct *P* arrival, with the use of the same records as the *PKKP* stack. No precursors are visible, verifying that the energy observed before *PKKP* is not an artifact of the stacking procedure. The increase in noise level starting near 100° results from the decrease in *P* amplitude as it diffracts around the outer core.

model underpredicts the observed power at short ranges and overpredicts the observed power at long ranges; indeed, the model fails in a formal statistical sense to fit the data within the estimated error bounds. Within the limitations of Kirchhoff theory, we have not been able to identify a model of CMB topography that reproduces the power versus range behavior of the observed precursors, which suggests contributions from scatterers elsewhere in Earth.

Forward scattering in the crust or mantle cannot account for energy arriving before *PKKP* at ranges less than 125° (Fig. 1). Backscattered energy from the lowermost mantle heterogeneity above the *PKKP* reflection points could, in principle, produce precursors, but it is unlikely that these would have the necessary power (6), and their amplitudes would probably exhibit a range dependence similar to that predicted for CMB topography.

Scattering within the liquid outer core is unlikely, as there is no evidence for lateral velocity or density variations within the outer core, which is consistent with a well-mixed, vigorously convecting layer. However, scattering might be possible from the solid inner core, where observations have indicated that lateral heterogeneity and anisotropy are present (*24*). Ray-tracing calculations show that energy scattered along the *PKKPdf* ray path within the outermost inner core or at the inner core boundary (ICB) arrives at times consistent with the observed precursors (Fig. 3). However, large scattering angles of 90° or more are required to explain the precursor onset times. The predicted amplitude of the direct *PKKPdf* phase is less than that of *PKKPab* and *PKKPbc*, owing to a small reflection coefficient at small CMB incidence angles and large inner core attenuation. Indeed, this and previous studies have not revealed a single observation of this phase (*25*). Predicted *PKKPdf* power in our synthetics is ~100 times smaller than the power level of the observed precursors when inner core attenuation is included, increasing to five times the level of the precursors when attenuation is neglected. It might be possible to explain the absence of direct *PKKPdf* and produce observable scattered energy by assuming that some of the *P*-wave attenuation within the inner core is due to scattering. Strong scattering would be required to prevent observation of a coherent *PKKPdf* arrival, and lowering of the intrinsic attenuation would be necessary to produce observable scattered energy. The large scattering angles and the lack of a direct arrival suggest that Kirchhoff and Born scattering theories are not applicable and a multiple scattering theory will be required to accurately test such a scenario.

The possible existence of scattering contributions from sources other than the CMB does not preclude the placement of upper bounds on its topography. The tightest bounds are obtained at a distance range of 106°, because of the low noise level and higher predicted precursor/*PKKP* power ratios at longer ranges. Short-wavelength topography will scatter more high-frequency energy, resulting in a smaller bound for lower values of λ. The topography is bounded at σ = 315 m for λ = 10 km, and σ = 630 m for λ = 20 km (Fig. 4). Such bounds are generous compared to the previously reported values of σ = 100 to 200 m for λ = 10 to 20 km from the Norwegian Seismic Array observations (6). However, our results were obtained by bounding the entire precursor wave train rather than bounding only a short time interval (1 to 5 s) before the main *PKKP* arrival.

The precursors are visible in stacks obtained from several spatially restricted subsets of the data, which suggests that they are a global phenomenon and are not restricted to a single anomalous source-receiver path.

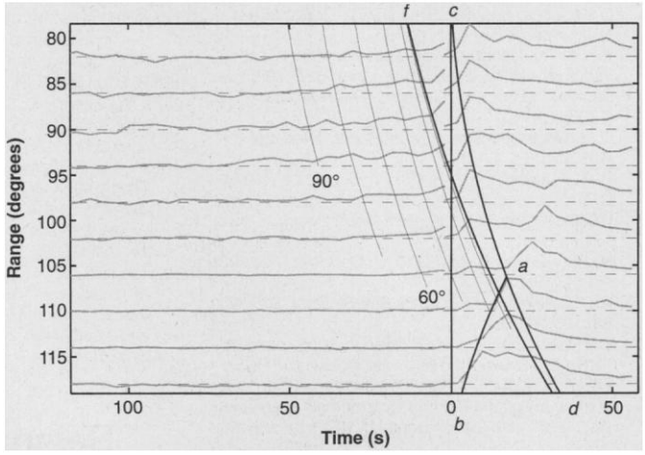

Fig. 3. *PKKP* data stacks and minimum travel time curves for scattering at the ICB. The data stacks (thick gray lines) are normalized to the maximum trace power and magnified eight times starting 2 s before the predicted arrival time (thin dashed lines indicate zero values). Travel times for the *PKKPab*, *PKKPbc*, *PKKPcd*, and *PKKPdf* branches are shown as wide solid lines, with different branches labeled in lowercase italics. The thin solid lines are the minimum travel time for energy scattered at the second or third ICB crossing point for angles from 15° to 90° at 15° intervals. Contributions from single scattering at the ICB would require large scattering angles, up to 90° to match the onset of precursor energy. There is no clear indication of a *PKKPdf* arrival in the observations. *PKKPab* extends well beyond the ray-theoretical limit of 106° (*27*), a result of the tunneling effect (*28*), and its amplitude exceeds that of *PKKPbc*, a result of an increased reflection coefficient at shallower reflection angles.

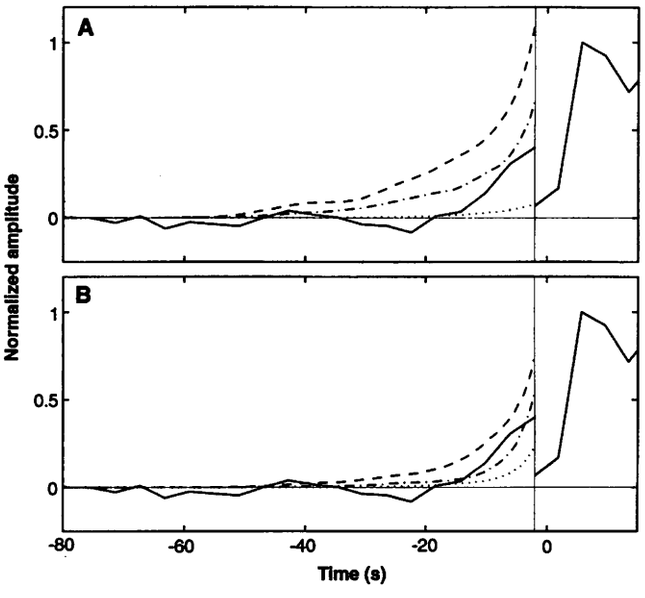

Fig. 4. Predicted scattering envelopes for topography with a fixed scale length λ and different rms amplitudes σ. (**A**) Solid line, data stack and predictions for λ fixed at 10 km; dashed line, predictions for σ = 450 m; dashed-dotted line, predictions for σ = 315 m; and dotted line, predictions for σ = 100 m. (**B**) Solid line, data stack and predictions for λ fixed at 20 km; dashed line, predictions for λ = 630 m; dashed-dotted line, predictions for σ = 450 m; and dotted line, predictions for σ = 300 m. The predicted envelopes bound the observed precursors (both shown magnified six times) at σ = 315 m for λ = 10 km and σ = 630 m for λ = 20 km. In general, changing σ scales the amplitude of the synthetic precursor envelope and has a secondary effect on its shape, whereas changing λ affects both its shape and amplitude, with longer wavelength topography producing scattered energy concentrated closer to the *PKKP* arrival.

However, the partitioning of the waveforms in our data set increases the variance of the observations, currently limiting the ability of this approach to resolve lateral variations in scattering strength.

REFERENCES AND NOTES

1. A. M. Dziewonski and D. L. Anderson, *Phys. Earth Planet. Inter.* **25**, 297 (1981).
2. D. E. Loper and T. Lay, *J. Geophys. Res.* **100**, 6397 (1995).
3. A. Morelli and A. M. Dziewonski, *Nature* **325**, 678 (1987).
4. J. Neuberg and J. Wahr, *Phys. Earth Planet. Inter.* **68**, 132 (1991); A. Rodgers and J. Wahr, *Geophys. J. Int.* **115**, 991 (1993); R. J. Pulliam and P. B. Stark, *J. Geophys. Res.* **98**, 1943 (1993); P. B. Stark and N. W. Hengartner, *ibid.*, p. 1957.
5. W. Menke, *Geophys. Res. Lett.* **13**, 1501 (1986); J. Vidale and H. M. Benz, *Nature* **359**, 627 (1992); K. Bataille and F. Lund, *Geophys. Res. Lett.* **23**, 2413 (1996).
6. D. J. Doornbos, *Phys. Earth Planet. Inter.* **21**, 351 (1980).
7. R. A. Haddon and J. R. Cleary, *ibid.* **8**, 211 (1974); D. J. Doornbos, *Geophys. J. R. Astron. Soc.* **53**, 643 (1978); K. Bataille *et al.*, *Pure Appl. Geophys.* **132**, 151 (1990).
8. K. Bataille and S. M. Flatte, *J. Geophys. Res.* **93**, 15057 (1988).
9. A. C. Chang and J. R. Cleary, *Bull. Seismol. Soc. Am.* **68**, 1059 (1978).
10. Our data, spanning 1988 through 1995, were obtained by means of the IRIS Fast Archive and Recovery Method (FARM). The FARM database contains shallow events (<100 km) with moment magnitude (M_w) ≥5.8 and deep events (>100 km) with M_w ≥5.5.
11. P. S. Earle and P. M. Shearer, *Bull. Seismol. Soc. Am.* **84**, 366 (1994); L. Astiz *et al.*, *Seismol. Res. Lett.* **67**, 8 (1996).
12. Including seismograms with impulsive noise bursts resulting from unrelated earthquakes or instrument error would contaminate the stacked image. Seismograms containing such artifacts were removed by visual inspection. In addition, possible contamination from double events was further avoided by removing traces with impulsive energy arriving before the theoretical *P* arrival. Other seismic phases, including *SS*, *SP*, and *SPP*, overlap a portion of the time-distance window in which the precursors were imaged. However, these phases have a different move-out and are not consistently observed at high frequencies (*11*) because of the high attenuation of the *S* phase.
13. Eighty-nine percent of the CMB is within 10° of a *PKKP* underside CMB reflection point. However, 83% of the reflection points are in the Southern Hemisphere, due to a concentration of seismic stations in the Northern Hemisphere.
14. E. R. Kanasewich, *Time Sequence Analysis in Geophysics* (Univ. of Alberta Press, Alberta, Canada, 1981).
15. We subtracted the average noise from a 60-s window starting 140 s before the *PKKPbc* arrival. Shifting the noise window to a time that overlaps with the precursory wave train changes the precursors' zero offset but not their shape.
16. The maximum amplitude was taken from the processed trace in a 15-s window starting at the theoretical *PKKPbc* arrival time.
17. The weight assigned to a processed trace was defined as the ratio of the maximum value found in a signal window to that taken in a noise window. An incorrect choice for the position of the noise window can bias the amplitude of the precursors, highlighting the importance of the *P*-wave test (Fig. 2C). A gap between the end of the noise window and the start of the reference phase will falsely amplify the observed precursors by ~5%. This was verified in stacks using *P* as a reference phase. A false precursory wave train was imaged, for distance ranges with poor STN, when using a noise window ending 50 s before the *P* arrival time. A noise window that overlaps the precursory time window may reduce the amplitude of the observed precursors, down-weighting seismograms with large-amplitude precursors. This effect is negligible, given that the amplitude of the noise on a single trace is up to 10 times greater than that of the precursors. Thus, we use a 140-s noise window ending 5 s before *PKKPbc* and a 15-s signal window starting at the *PKKPbc* onset time. It is also possible for the stack to be biased by an anomalously large reference phase (possibly resulting from focusing effects); this was avoided by assigning a maximum weight of 7 to each individual trace. Although the choice of noise window and weighting scheme can influence the absolute level of the observed precursors, the relative amplitude of the *PKKPbc* precursors with range was independent of the choice of windowing.
18. The source-receiver range for deep events was corrected to its zero depth equivalent by ray tracing from the hypocenter to the surface with the use of the *PKKPbc* ray parameter.
19. B. Efron and R. Tibshirani, *Science* **253**, 390 (1991).
20. I. Tolstoy and C. S. Clay, *Ocean Acoustics: Theory and Experiment in Underwater Sound* (McGraw-Hill, New York, 1966); P. Scott and D. Helmberger, *Geophys. J. R. Astron. Soc.* **72**, 237 (1983); J. A. Ogilvy, *Theory of Wave Scattering from Random Rough Surfaces* (Institute of Physics, London, 1991).
21. W. Kampfmann and G. Müller, *Geophys. Res. Lett.* **16**, 653 (1989).
22. The extreme values for the grid search were $\lambda = 5$ to 30 km and $\sigma = 100$ to 1000 m. In general, increasing σ scaled the amplitude of the predicted precursory and increasing λ concentrated the energy near the *PKKPbc* arrival.
23. A model of CMB topography could not be found that fit our observations within their error bounds over the entire distance range, giving rise to the possibility of additional sources of scattering. Thus, limits were placed on the model parameters by consideration of models that matched the general character of the observations. Synthetics for $\lambda < 7$ km predict a precursory wave train that does not monotonically increase with time at shorter distance ranges, which is a result of the increased contribution of *ab*-to-*ab* scattering. Synthetics calculated for $\lambda > 10$ m concentrate the observed energy near the *PKKPbc* arrival.
24. G. Poupinet *et al.*, *Nature* **305**, 204 (1983); A. Morelli *et al.*, *Geophys. Res. Lett.* **13**, 1545 (1986); J. H. Woodhouse *et al.*, *ibid.*, p. 1549; P. M. Shearer and K. M. Toy, *J. Geophys. Res.* **96**, 2233 (1991); K. C. Creager, *Nature* **356**, 309 (1992); P. M. Shearer, *J. Geophys. Res.* **99**, 19647 (1994); W. J. Su and A. M. Dziewonski, *ibid.* **100**, 9831 (1995); X.-D. Song and D. V. Helmberger, *ibid.*, p. 9805.
25. E. R. Engdahl, thesis, Saint Louis University, St. Louis, MO (1968).
26. R. A. W. Haddon, *Eos* **53**, 600 (1972); M. Hedlin *et al.*, *Nature* **387**, 145 (1997).
27. E. R. Engdahl, *Science* **161**, 263 (1968).
28. P. G. Richards, *Geophys. J. R. Astron. Soc.* **35**, 243 (1973).

29. We thank the personnel from the IRIS-GSN stations for providing the data and specifically R. Benson for maintaining the FARM archive. This work benefited from the suggestions of B. Engdahl, two anonymous reviewers, and many co-workers and was supported by NSF grant EAR93–15060.

4 March 1997; accepted 5 June 1997

Seismic Evidence of Partial Melt Within a Possibly Ubiquitous Low-Velocity Layer at the Base of the Mantle

J. Revenaugh* and R. Meyer

Three source regions show evidence of a low-velocity layer that is less than 15 kilometers thick on top of the core-mantle boundary and require about a 3:1 ratio of shear-to-compressional velocity reduction, which is consistent with partial melt. Layer thickness is correlated with travel time residuals of the seismic phases that are most sensitive to the lowermost mantle velocity. These observations suggest that the layer is thinned beneath downwellings but is present everywhere along the core-mantle boundary. Low viscosity accompanying partial melt can localize the upwelling of warmed mantle, making the low-velocity layer a plausible source of mantle plumes.

Recent seismic work has mapped several anomalously slow regions of the lowermost mantle, taking the form of an ultra–low-velocity layer ≤40 km thick on top of the core-mantle boundary (CMB) (*1*, *2*). *P* wave velocity (v_P) within the layer is as much as 10% lower than that of the overlying mantle. Partial melt offers an explanation of the layer (*3*) and predicts a 30% shear wave velocity (v_S) drop within the layer (*3*, *4*). Because the CMB approximates an isotherm, this hypothesis also predicts layer ubiquity in the absence of substantial compositional heterogeneity. We tested these predictions by searching for reflections from the layer in seismograms recorded by California regional arrays.

PcP, the high-frequency compressional-wave reflection from the CMB, is often used to study the detailed structure of the boundary (*5*). Its typically low signal-to-noise ratio necessitates the use of array data to avoid misinterpretation of noise as an anomalous structure. Precursors to *PcP* due to reflection or scattering from lowermost mantle structures are further buried in noise (*2*, *6*). To detect them and measure their amplitude

J. Revenaugh, Institute of Tectonics, University of California, Santa Cruz, CA 95064, USA.
R. Meyer, Department of Geological Sciences, University of California, Santa Barbara, CA 93106, USA.
*To whom correspondence should be addressed.